MONMOUTH COLLEGE

UNDERGRADUATE THESIS

The Study of Insulin Aggregation, Dissociation, and Interactions at the Air-Water Interface

---

Author:
Seth CROSLOW

Supervisor:
Dr. Audra GOACH

A thesis submitted in fulfillment of the requirements for the degree of Bachelor of Science in Chemistry

in the

Goach Research Group
Department of Chemistry - Monmouth College

April 10, 2021

MONMOUTH COLLEGE

Abstract

Dr. Audra Goach
Department of Chemistry - Monmouth College

Bachelor of Science in Chemistry

The Study of Insulin Aggregation, Dissociation, and Interactions at the Air-Water Interface

by Seth CROSLOW

A holistic study of insulin at the air-water interface is herein reported. Using the Langmuir Monolayer Technique, the effect of pH at physiological temperature on the oligomeric state of insulin was tested by altering the pH of various subphases (water to induce monomeric/dimeric forms and a divalent metal cation salt to induce a hexameric form). The hexameric form of insulin is typically formed in the presence of zinc cations, however, the effects of other metal cations were tested on insulin at physiological pH and temperature. Each of the metal cations was also studied with each insulin's three conformations, T_6, T_3R_3, and R_6, to see how insulin's conformation affects its aggregation, interactions among hexamers, and overall stability. Two vanadium complexes ($VOSO_4$ and $NaVO_3$) were also studied to see if they could induce the hexameric form of insulin. Finally, a Brewster angle microscope was built and tested. This was used to visualize the topology of the insulin monolayers and identify any discernible features present as an additional method of distinguishing between the various insulin conformations and oligomeric forms.

Contents

List of Figures

List of Tables

List of Abbreviations

BAM	Brewster Angle Microscopy
CCD	Charge Coupled Device
CM	Compression Modulus
CV	Coefficient of Variation
DPPC	Dipalmitoylphosphatidylcholine
DPPS	1,2-dipalmitoyl-sn-glycero-3-phospho-L-serine
EDTA	Ethylenediaminetetraacetic Acid
HI	Human Insulin
HINS	Human Recombinant Insulin
LMA	Limiting Molecular Area

Chapter 1

Introduction

1.1 Langmuir Monolayer Technique

1.1.1 Background

The history of the Langmuir Monolayer technique–in addition to that of surface science in general–dates back to the eighteenth century, when Benjamin Franklin observed that the waves of a lake were calmed due to accidentally thrown-out greasy water.[1] During his experiments, Franklin noted that oil spreads out while at an air-water interface, however, does not at the air-granite interface.[2] Oils and other surfactants–molecules that reduce the surface tension of water–orient at the air-water interface due to their ampipathic nature:one side of the molecule is hydrophobic and another is hydrophilic.[3] These molecules self-orient at the air-water interface as a way to reduce unfavorable interactions with their hydrophobic side orienting upwards to the air and their hydrophilic side sinking into the water; all of the molecules eventually do this forming a monolayer.[3] Lord Rayleigh further investigated this event and calculated that the oil spread to a thickness of about 1.6 nm, similar to the current predictions of the time for a mono-molecular film.[4] Later, Agnes Pockel, a German scientist who had been studying area of oil in her kitchen sink and developed a device to do so, heard of Rayleigh's research, and the two published a paper together.[5]

This research set a precedence for Irving Langmuir's research where he improved on

Pockel's trough and created his own *Langmuir Trough* (shown in *Figure 1.1*). This design utilized a balance mechanism (*K*) to measure the surface tension of oil spread on a water surface (*T*). Two glass rods (*R and R'*) hang down onto a piece of paper (*B*). As the barrier (*A*) is pushed forward, the oil starts to exert a force on the paper; when the paper (*B*) is directly under point (*J*), the force exerted by the surface tension of the oil is proportional to the weight in the balance (*P*). Multiple weights are used, and the distance of (*A*) verses the derived surface tension were then plotted to obtain a surface tension-area plot.

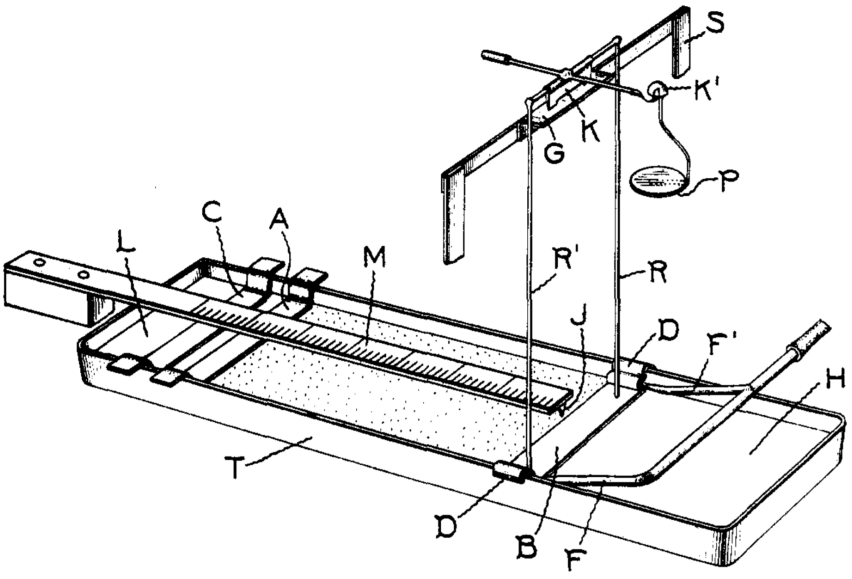

Figure 1.1: Initial trough design by Irving Langmuir for measuring surface tensions of oil spread at the air-water interface.[6]

The surface tension on a liquids surface, such as the oil resting on the surface of the water, arises due to an imbalance in the forces between the atoms in the liquid. These forces, also known as surface free energy, can be quantified using this method, and are expressed in terms of mN/m. In current Langmuir troughs, an electrobalance is used to

measure the force exerted on a probe or plate by the subphase and surfactant (*shown in Figure 1.2*). The total forces exerted on a Wilhelmy plate is shown in *equation 1.1*.

$$F = Weight - Normal\ Force + Surface\ Tension \tag{1.1}$$

This equation can be be expressed in terms of measurable quantities, as shown in *equation 1.2*.

$$F = \rho gLWt - \rho' ghWt + 2\gamma(t + W)cos\theta \tag{1.2}$$

where L,W and t are the length, width and thickness of the probe; h is the immersed depth of the probe; γ is the surface tension of the liquid; ρ' is the density of the subphase; and θ is the contact angle of the probe.

The surface pressure of a system can be calculated by taking the difference in surface pressures with and without an added monolayer film (shown in *equation 1.3*).

$$\pi = \gamma_0 - \gamma \tag{1.3}$$

where π is the surface pressure of the film, γ_0 is the surface tension of the subphase (72.8 mN M^{-1} for water), and γ is the surface tension of the subphase with a monolayer.

1.1.2 Surface Pressure-Area Compression Isotherm

The characteristic method of representing this data is through a surface area-pressure compression isotherm. In this plot, phase changes within the monolayer can be viewed as changes in the slope of the resulting line. Towards the bottom of the graph, the monolayer exists in a gaseous state (G). As the mean molecular area decreases, the film shifts to

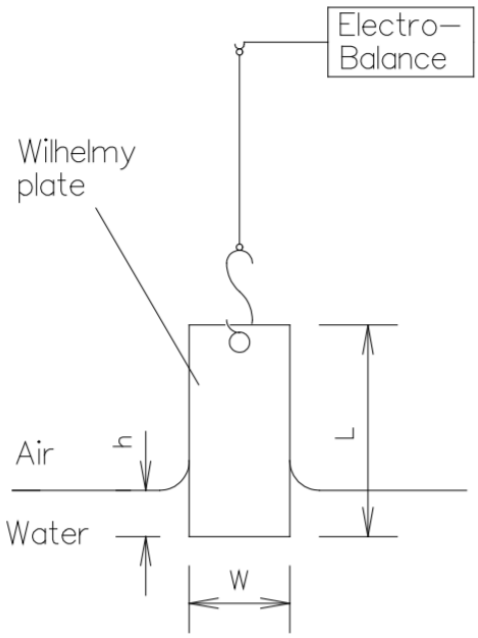

Figure 1.2: Setup for Langmuir trough using a Wilhelmy plate.

a liquid expanded (LE), liquid (L), liquid condensed (LC), then solid state (S). After the solid state, the monolayer collapses (C) indicated by the horizontal/decreasing slope. The limiting molecular area (LMA), which is the smallest area to which the monolayer can be compressed, is found by extrapolating the largest slope (S) to the x-axis.

The different phases of the monolayer indicate the relative fluidity and compactness of the monolayer.[7] In addition to using a surface pressure-area compression isotherm, other optical techniques can be used to assess the phase of the monolayer including Brewster angle microscopy[8–10] and fluorescence microscopy.[11–13] Both of these optical techniques directly visualize the phases of the monolayer as intensity of light: the brighter the region, the more compressed the monolayer is and the higher phase it is in (i.e. solid or liquid condensed).

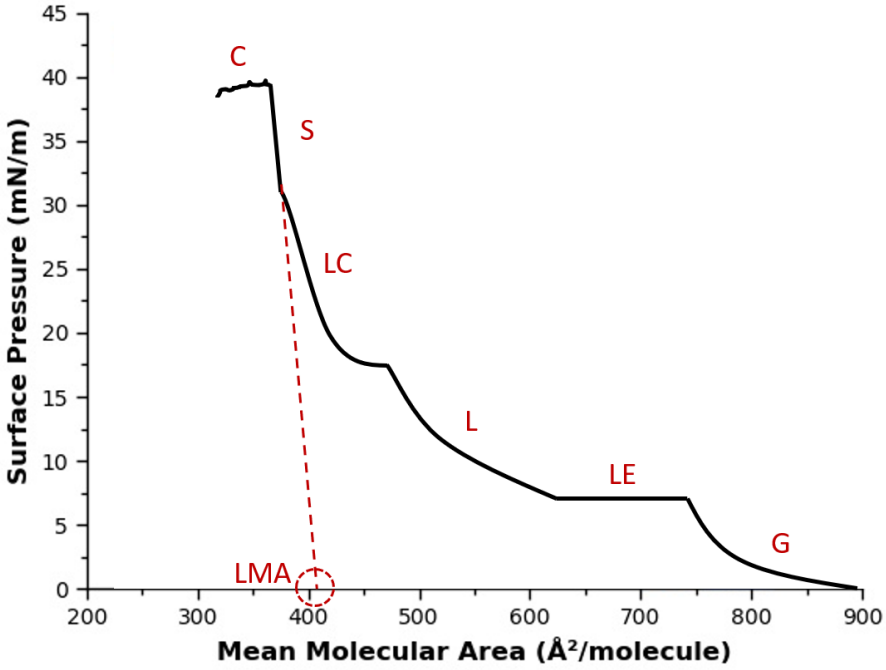

Figure 1.3: General structure of a surface pressure-area compression isotherm.

1.1.3 Compression Modulus

In addition to simply viewing the monolayer or assuming the phase of the monolayer base on the transitions, a mathematical approach is available to calculate the phase of the monolayer. This calculation, called the compression modulus, results in a value of how compressible the monolayer is, and, therefore, its phase. The calculation for the compression modulus from the surface pressure-area compression isotherm data is shown below:

$$Cs^{-1} = -A(\frac{\partial \pi}{\partial A}) \tag{1.4}$$

where Cs^{-1} is the compression modulus, A is the area of the monolayer, and π is the surface pressure.

The corresponding phases for each compression modulus value is shown in Table 1.1

Compression Modulus (mN/m)	**Phase of Monolayer**
<12.5	Gas
12.5-50	Liquid Expanded
50-100	Liquid
100-250	Liquid Condensed
>250	Solid

Table 1.1: The compression modulus values that correspond to each phase of the monolayer

1.1.4 Ideal Mixing

In general, the Langmuir monolayer technique is used to study simplistic models that represent a type of cell membrane. These models can be simply a single compound to study how it undergoes phase changes during compression. They can also be more complicated models where multiple surfactants are added to see how they interact with each other. In this case, an ideal mixing algorithm is useful to asses how the surfactants are interacting. The miscibility of two surfactants can be calculated using the ideal mixing equation below:

$$A_I = (A_1)(X_1) + (A_2)(X_2) \tag{1.5}$$

where A_I is the ideal area of the mixture, A_x is the area of an individual surfactant, and X_x is the mole fraction of the surfactant in the mixture.

Once the ideal area of the mixture is calculate the excess of the average area per molecule can be calculated using the following equation:

$$A_E = A_{1,2} - A_I \tag{1.6}$$

where A_E is the excess area per molecule of the mixture, $A_{1,2}$ is the actual area of the mixture, and A_I is the ideal area of the mixture calculated above.

If the A_E is zero, the surfactants are not interacting and are mixing immiscibly; this is known as ideal interaction.[14] However, if the A_E diverges away from zero, the surfactants are interacting and mixing miscibly; this is known as a non-ideal interaction. If the A_E is negative, the two surfactants have a condensing effect on each other.[15] If the A_E is positive, the two surfactants have an expanding effect on each other. The deviation from the ideal isotherm is typically reported as a percent difference as a whole, or at a surface pressure of 30 mN/m (the surface pressure at which the Langmuir monolayer model most resembles a real cell membrane).

Additonally, from the ideal mixing isotherm, the Gibbs free energy of mixing–which summarizes all of the deviations from an ideal interaction, including the entropic and enthalpic effects of the mixture[16]–can be calculated using the following equation:[17]

$$G^E = \int_0^\pi A_E d\pi \tag{1.7}$$

where G^E is the excess Gibbs free energy, π is the surface pressure, and A_E is the average excess area per molecule of the mixture.

1.2 Insulin

1.2.1 Insulin Production

Insulin is a polypeptide hormone that is produced in the β-cells in the Islets of Langerhans in the pancreas. It is initially produced as preproinsulin which contains an additional signaling polypeptide extension. The signal polypeptide chain is then cleaved to form proinsulin in the rough endoplasmic reticulum. Finally, the proinsulin folds, forming three disulfide bonds and the c-chain is cleaved in the Golgi apparatus.[18] This process is summarized in Figure 1.4

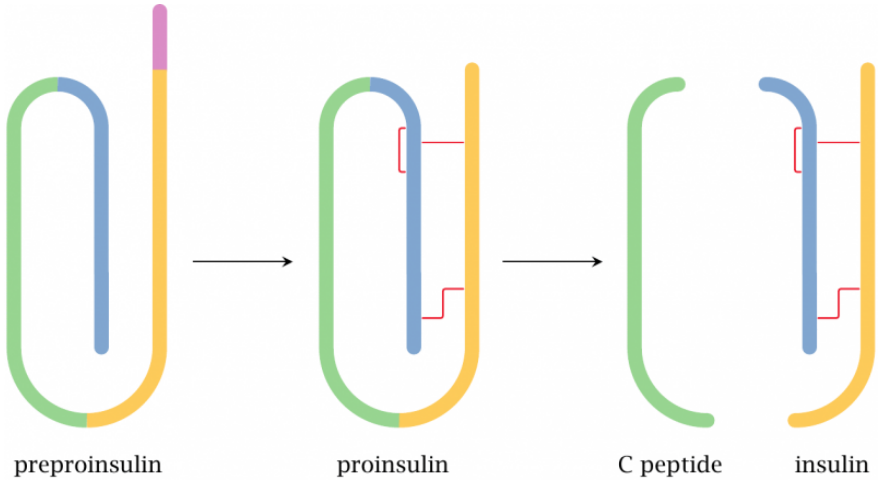

Figure 1.4: Formation of insulin from preproinsulin[19]

1.2.2 Insulin Monomer Structure

In its monomeric form, insulin contains two chains: a 21 residue, hydrophobic A-chain and a 30 residue, hydrophilic B-chain.These two chains are connected to each other via

two disulfide bonds, with another disulfide bond occurring in the A-chain.[20] The full amino acid sequence for the insulin monomer structure is shown in Figure 1.5. Since the insulin monomer contains both a hydrophobic and hydrohpilic part (and is, therefore, amphiphilic) it can self orient at the air-water interface and form a monolayer. The A-chain of insulin is comprised of two -helical segments, and the B-chain consists of an α-helix center with two β-turns on either side.[21]

1.2.3 Insulin Oligomer Structures

Insulin exists in several oligomeric forms in solution including most notably the monomer, dimer, and hexamer. Within the body, insulin is typically stored in the hexameric form due to its increased stability compared to the other oligomeric forms. To be used by the body, the hexamer dissociates into the dimer, then the monomer, which is readily used within the body. These insulin monomers can adopt two different states: the "tense" state, T, or the "relaxed" state, R. In the tense state, the amino acid residues B1-B8 are extended.

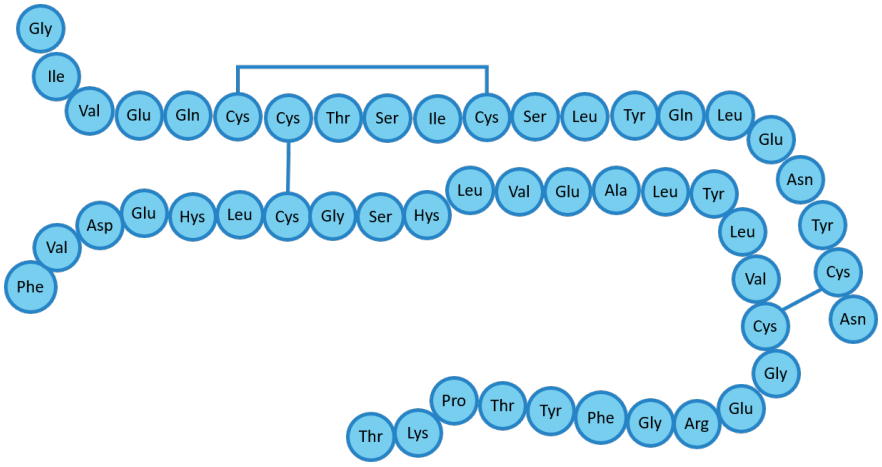

Figure 1.5: Insulin monomer amino acid sequence

However, in the relaxed state, these amino acid residues adopt an α-helical structure.[21] In solution, one insulin monomer forms four hydrogen bonds with another to produce a dimer.[22]

In the presence of a divalent transition metal cation, typically Zn^{2+}, insulin favors the hexameric conformation. The insulin hexamer, due to the two forms of the monomer, has several conformations as well. The three main conformations, stemming from the T and R states of the monomers, are the T_6, T_3R_3, and the R_6 conformations.[23] Each of these conformations are produced through a combination of a metal cation, anion, and a phenol: T_6 (Zn^{2+}), T_3R_3(Zn^{2+} and Cl^-), and the R_6 (Zn^{2+}, Cl^-, and phenol).[24] The experimentally determined structures of the three conformations of the insulin hexamer are shown in Figure 1.6. Other metals (mainly copper) have been tested to see if they too will induce the insulin hexamer form; these new hexamers are denoted with a prime (i.e. T_6').

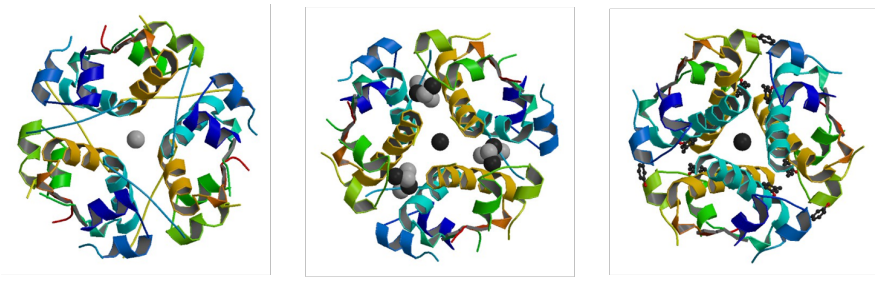

Figure 1.6: Structures of the three insulin hexamers including the PDB file number.

1.3 Brewster Angle Microscopy

Brewster angle microscopy utilizes simple optical mechanisms in order to visualize films on surfaces at an interface (typically air-water). Brewster studied light at many interfaces and noticed that incident unpolarized light could become polarized;this unpolarized light becomes reflected and refracted.[25] This phenomenon can be described by Snell's law:

$$n_1 sin\theta_1 = n_2 sin\theta_2 \tag{1.8}$$

where n is the index of refraction of the medium and θ is the angle that light makes with respect to the normal of the surface (θ_1 is the incident and reflected light angle and θ_2 is the refracted light angle).

Rearranging Equation 1.8, results in the following equation:

$$\frac{n_2}{n_1} = \frac{sin\theta_1}{sin\theta_2} \tag{1.9}$$

For a special case when the angle between the reflected and refracted light is 90, Equation 1.9 reduces to Brewster's Law since θ_2=θ_1+90, thereby reducing the sinθ_2 into cosθ_1 and the entire fraction to tanθ_1:

$$tan\theta_1 = \frac{n_2}{n_1} \tag{1.10}$$

This new angle, known as Brewster's Angle, reflects only s-polarized light (light that is perpendicular to the plane of incidence) and refracts only p-polarized light (light that is parallel to the plane of incidence. Due to this complete polarization, when strictly p-polarized light is incident on a surface, no light will be reflected. This is the main principle behind Brewster angle microscopy: in the absence of a surfactant, no light will be reflected

from the surface, however, in the presence of a surfactant, light will be reflected due to a change in the index of refraction on the medium. This process is demonstrated in Figure 1.7.

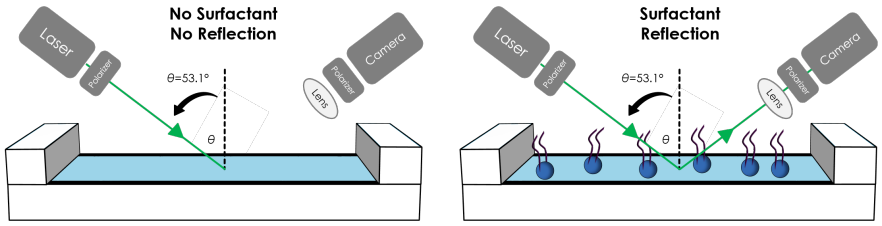

Figure 1.7: General Brewster angle microscopy principle for Langmuir monolayers

Due to the fact that BAM uses only incident light to determine film morphology, it is typically regarded as being superior to other optical methods since it does not a probe to be placed into the film or directly onto the surfactant of interest (as is the case with fluorescence microscopy).[26] This technique allows for the visualization of film inhomogenieties (differences in film phase) as well as for the determination of film thickness.[27]

Chapter 2

Insulin Aggregation

2.1 Introduction

Human insulin (HI) is a biologically active polypeptide molecule that is responsible for the regulation of blood glucose levels.[18,28] HI is produced and stored in the β-cells of the pancreas and is released into the bloodstream in response to various stimuli, primarily high blood glucose levels.[29] Human insulin is constructed from two polypeptide chains linked via two interchain disulfide bridges; the hydrophobic A-chain consists of 21 residues and the hydrophilic B-chain consists of 30 residues.[28] Within the body, two native HI monomers dimerize with each other at the C-termini of the B-chains via hydrogen bonding.[30] HI monomers can also aggregate to form larger oligomers, the most stable being the hexamer.[31,32] The structure of the HI hexamer has been widely studied using X-Ray crystallography and is shown to consist of either three HI dimers or two HI trimers coordinated around 2-4 Zn^{2+} ions.[33–35]

The overall structure of the insulin hexamer depends vastly upon the addition of allosteric effectors, such as anions and phenol derivatives. When the insulin hexamer is introduced to these, its structure changes to allow for new binding sites and pockets to form.[36] The conformations associated with the addition of these allosteric effectors are termed the T_6, T_3R_3, and the R_6 conformations with regards to the state in which each of the six monomers resides (T vs R).[32,37] In order to induce these conformations, insulin

must be in the presence of Zn^{2+} (T_6); Zn^{2+} and Cl^- (T_3R_3); and Zn^{2+}, Cl^-, and a phenol derivative (R_6).[38,39] The two states, tense (T) and relaxed (R), are classified using the structure of the first eight amino acids within the B-chain. In the T state, the eight amino acids are extended, whereas, in the R state, they are helical.[34] Additional divalent metal cations, mainly copper and cobalt, have been researched and found to also induce these hexameric conformations.[40–42]

The Langmuir monolayer technique has been widely used to model biological systems and attain information regarding the fluidity of the system as well as to see how the membrane interacts with other compounds.19-23 Several studies have been performed on insulin using this technique to study the stability of insulin, its aggregation equilibrium, and also how it is affected by changes in environmental conditions such as pH and temperature.24-26 Though several aspects of insulin have been studied using the Langmuir monolayer technique, there has yet to be a holistic study of the stability of the various conformation of the insulin hexamer or how various metal cations affect the stability of the hexamer.

2.2 Materials and Methods

2.2.1 Solution Preparation

Human insulin (human recombinant, MW 5808), $ZnSO_4$, $ZnCl_2$, $CuSO_4$, $CuCl_2$, and phenol were all obtained from Sigma-Aldrich (St. Louis, MO, USA). INSERT VANADIUM PLACE. Solutions of human insulin (HI) (1.50 mg/mL) were made by dissolving HI in 0.06 M HCl, and kept under refrigeration at 4 °C. All monolayer subphases for the Langmuir trough were made by adding each reagent (1 mM) into water then adjusting the pH

Trial	LMA (A^2/Molecule)	CM (mN/m)	CV
pH 3.3	268.799	72.374	0.054
pH 5.3	225.407	64.020	N/A
pH 7.4	261.528	72.365	0.04

Table 2.1: Quantitative data interpolated from the area-pressure compression isotherms for insulin on water.

to 7.4 using 1M HCl or NaOH. All solutions and subphases were made using ultrapure water (resistivity 18.2 M·cm, 25 °, Millipore). Vanadium solutions were prepared first by lowering the pH of water to 3, adding the vanadium compound, then slowly raising the pH to 7.4 using NaOH.

2.2.2 Langmuir Monolayer Film Preparation

Insulin monolayers were created by depositing 8.0 L of insulin solution (1.5 mg/mL) onto the aqueous subphases described previously. The film was allowed 10 min before compression to orient and form a monolayer. Compression isotherms were performed using a Kibron Microtrough G1 (surface area of 208 cm^2) with a compression speed of 40 A^2/molecule/min. The temperature of the subphase was maintained at 37 °C through the use of an external circulating water bath.

2.3 Results and Discussions

2.3.1 Insulin on Water

Figure 2.1 depicts surface pressure-area isotherms for HI on a water subphase as various pH. The isotherms at the isoelectric point of insulin (5.3) as well as at physiological

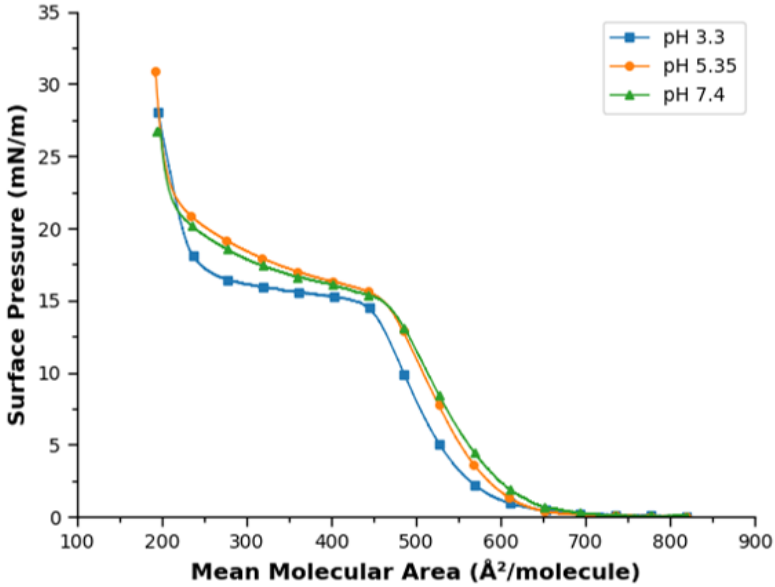

Figure 2.1: Surface Pressure-Area Isotherms Showing the Effect of pH on Insulin on a Water Subphase

pH (7.4) have nearly indistinguishable phase transitions. This indicates that similar interactions are occurring at these pHs despite the fact that insulin is negatively charged at physiological pH and overall neutral at its isoelectric point. At pH 3.3, however, the liquid expanded phase transition (pre-plateau) compresses slightly to a smaller molecular area and experiences a decrease in the surface pressure of the plateau region (15 vs 18 mN/m).

Nieto-Suárez et al. showed a decrease in the molecular area at which the liquid expanded transition begins when comparing pH 3.0 and 5.7 trials of insulin on water at 25 °C.[43] Their compression isotherm of insulin at pH 3.0, however, lost the plateau region where both the liquid expanded and liquid condensed phases coexist within the monolayer and had higher collapse pressures. The plateau and collapse pressures discrepancy

between the data presented here and that of Nieto-Suárez et al. could be explained due to a difference in temperature and compression speed. The same study by Nieto-Suárez et al. showed that at higher temperatures, the plateau region becomes more prominent and horizontal and at lower compression rates the collapse pressure decreases. The decrease in the liquid-expanded and plateau region in our data suggests that there are some unfavorable interactions occurring that might be due to the overall positive charge of the insulin molecule.

2.3.2 Insulin on $ZnCl_2$

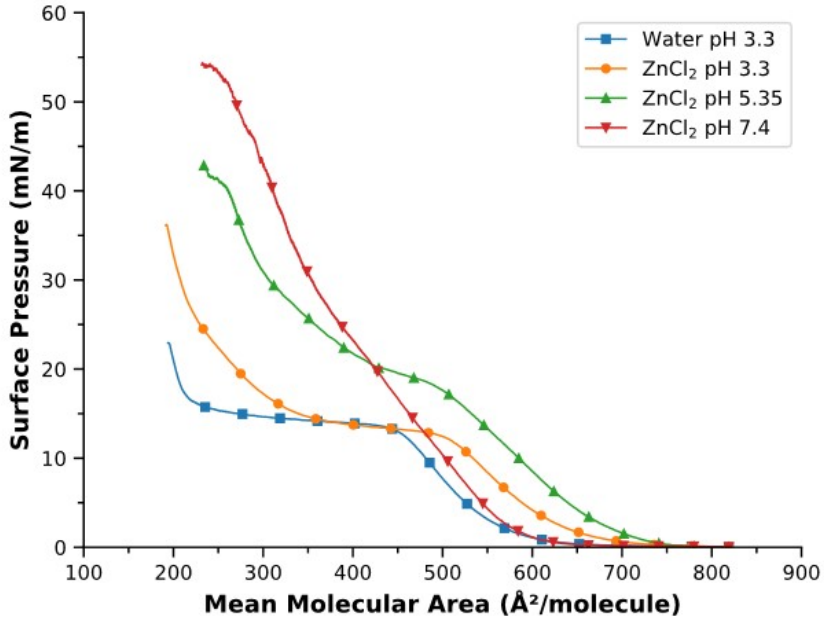

Figure 2.2: Surface Pressure-Area Isotherms Showing the Effect of pH on Insulin on a 1mM $ZnCl_2$ Subphase

Trial	LMA (A^2/Molecule)	CM (mN/m)	CV
Water pH 3.3	268.799	72.374	0.054
$ZnCl_2$ pH 3.3	267.957	97.545	0.075
$ZnCl_2$ pH 5.35	255.435	106.719	0.034
$ZnCl_2$ pH 7.4	425.715	98.529	0.006

Table 2.2: Quantitative data interpolated from the area-pressure compression isotherms for insulin on $ZnCl_2$.

Upon the addition of zinc, the insulin monomers/dimers adopt a hexameric conformation. Figure 2.2 shows the results of altering the pH of the T_3R_3 form of the HI hexamer with zinc. This figure contains a graph of insulin on water pH 3.3 for comparison to the monomeric/dimeric form of insulin. Since the insulin hexamer binds to zinc through histidine residues, below the pKa of histidine (6) where it is protonated and can no longer coordinate to the zinc, the hexameric form of insulin should not be present. This is shown in Figure 2.2 most prominently at pH 5.3 as it has lift-off area, LE phases transition, and a LE/LC plateau region similar to the monomeric/dimeric HI. While the insulin on $ZnCl_2$ trial at pH 5.3 highly resembles the overall shape of the insulin on water trails, the surface pressure of the LC/LE plateau as well as the collapse pressure are both higher.

A similar result was expected for the pH 3.3 trial of insulin on $ZnCl_2$, however at this lower pH the isotherm loses most of the LE/LC plateau and has a large increase in slope throughout the isotherm. The limiting molecular area, calculated by extrapolating the maximum slope of the isotherm to a surface pressure of 0 mN/m, for the pH 3.3 trial is nearly identical to that of the insulin on water trial (268 and 269 A^2/molecule, respectively). Lord et al. reported that at certain pH values (2.0 and 3.5) the presence of zinc does not change the circular dichroism (CD) spectrum[44] and also reported various studies that showed no difference between zinc-free insulin and insulin at a pH below 4.

Given that the CD spectrum showed no variance with and without the presence of zinc, the secondary structure of the insulin should be the same. This indicates that the increase in slope and loss of LE/LC plateau are most likely due to ionic interactions between insulin molecules from their overall positive charge.

The pH 7.4 graph in Figure 2.2 shows a similar liftoff area as compared to the other pH trials, however once this phase transition begins, it continues without another substantial phase transition until its collapse around 55 mN/m. The limiting molecular area for this pH is much larger than the other pH trials (425 vs 255-270 A^2/molecule). This nearly two-fold increase in limiting molecular area indicates the presence of aggregates, most notably the hexamer. Liu et al. obtained similar compression isotherms for insulin on 1 mM $ZnCl_2$ and used infrared reflectionabsorption spectroscopy to determine the orientation and secondary structure of insulin at the air-water interface and determined that in the presence of $ZnCl_2$ the hexamer is the main oligomeric form present.[20] They also proposed an orientation of the insulin hexamer at the interface where the B-chain of one of the dimers in the hexamer becomes submerged into the subphase and orients the rest of the hexamer into the air. Given this, it can be said with relative certainty that the compression isotherm shown in Figure 2.2 at pH 7.4 indicates the presence of the insulin hexamer.

2.3.3 Insulin on $CuCl_2$

The copper-substituted insulin hexamer has been minimally investigated. Gavrilova et al., however, showed that insulin is not purely selective to zinc and performed experiments that determined the dissociation constants of insulin monomers to zinc and copper.[40] This study found that the dissociation constant for copper is an entire order of magnitude

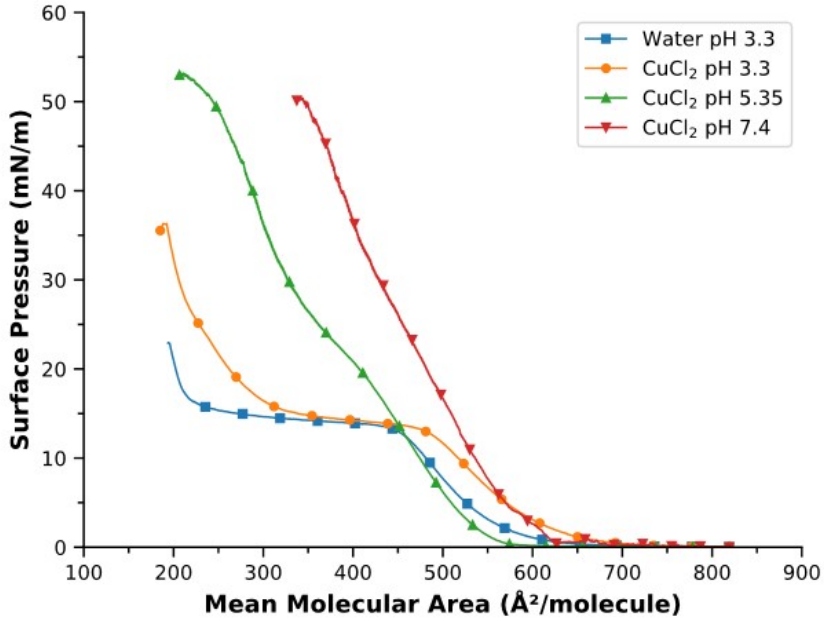

Figure 2.3: Surface Pressure-Area Isotherms Showing the Effect of pH on Insulin on a 1mM $CuCl_2$ Subphase

smaller (0.4 μM for zinc and 0.025 μM for copper), which indicates that the insulin has a higher affinity towards copper than towards zinc.

Figure 2.3 shows compression isotherms of insulin on a $CuCl_2$ under different pH values. The pH 3.3 data mimics the same data of insulin on $ZnCl_2$, however, the plateau region is slightly longer reducing the area at which the LC phase transition occurs. The pH 5.3 data shows a stark difference as compared to the pH 5.3 data on $ZnCl_2$ as it shows no plateau region and instead mimics the pH 7.4 data, though with a less steep slope. The pH 7.4 data in Figure 2.3 shows similar liftoff areas, phase transitions, and collapse pressures when compared to the data in Figure 2.2. This indicates that the copper was most likely able to induce the hexameric form of insulin. However, this data shows a larger limiting molecular area (470 vs 420 A^2/molecule) and has much higher compression modulus

Trial	LMA (A^2/Molecule)	CM (mN/m)	CV
Water pH 3.	268.799	72.374	0.054
CuCl2 pH 3.3	266.407	84.908	0.048
CuCl2 pH 5.35	476.918	67.084	0.050
CuCl2 pH 7.4	470.588	141.214	0.013

Table 2.3: Quantitative data interpolated from the area-pressure compression isotherms for insulin on $CuCl_2$.

value (140 vs. 100). This suggests that the copper-substituted insulin hexamer may be more expanded and order more tightly at the air-water interface.

2.3.4 Insulin on Vanadium

2.3.4.1 Vanadium Speciation

Vanadium exists in a variety of oxidation states based on various conditions, primarily pH. These oxidation states contain different amounts of vanadium per molecule, different overall charge, vastly different properties, and exhibit several different colors. The speciation of vanadium compounds under various pH conditions is shown in Figure 2.4.

2.3.4.2 Vanadium Isotherms

Area-pressure isotherms for two vanadium compounds, $VOSO_4$ and $NaVO_3$, are shown in Figure 2.5. The vanadyl sulfate ($VOSO_4$) isotherm shows seemingly hexameric characteristics as noted by its sharp phase transition around 1,300 A^2/molecule and lack of a prominent liquid expanded-liquid condensed plateau region, though there is a slight transition around 20 mN/m. Since the vanadyl molecule has a net positive charge of +2, similar to that of zinc and copper, it makes since that this molecule would induce the hexameric conformation of insulin.

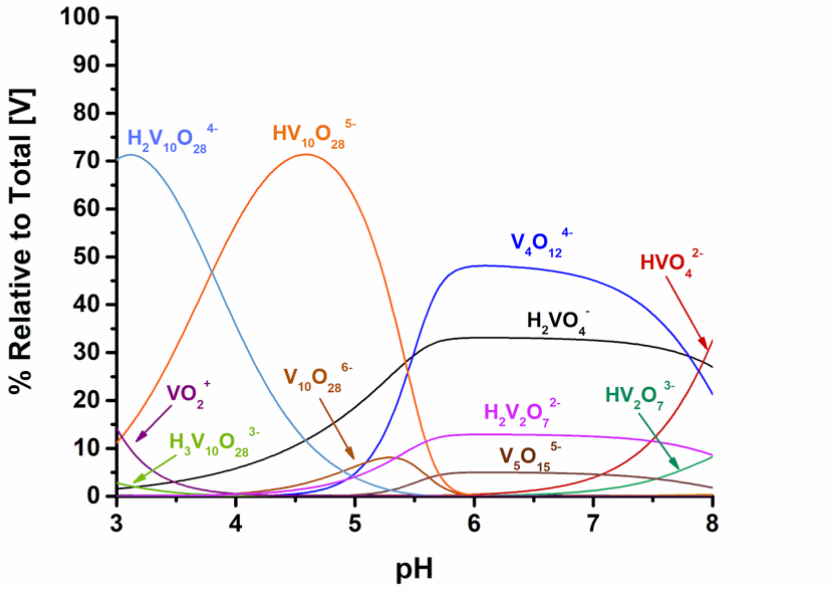

Figure 2.4: Vanadium speciation under various pH conditions with 1 mM vanadium concentration at 25 degrees Celsius. Speciation was calculated and provided by Cameron Van Cleave working under Dr. Debbie Crans at Colorado State University.

The isotherm of sodium metavanadate ($NaVO_3$), as shown in Figure 2.5, shows a potentially monomeric/dimeric conformation as indicated by the presence of a liquid expanded-liquid condensed plateau region beginning around 1,000 A^2/molecule. When comparing to the insulin on water isotherm, however, it is clear that the plateau region occurs at a higher surface pressure indicating that this insulin monomer/dimer is more stable, which is also validated by the increased collapse pressure of the sodium metavanadate. As sodium metavanadate has an overall charge of minus one, it is logical that it would not induce the insulin hexamer.

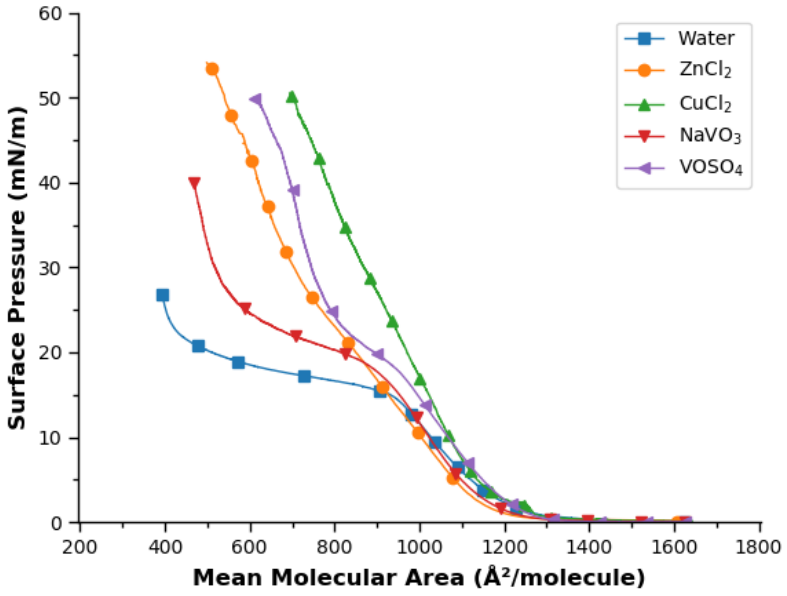

Figure 2.5: Comparison of $VOSO_4$ and $NaVO_3$ insulin aggregation to that of $ZnCl_2$ and $CuCl_2$. All trials were ran in 1 mM concentrations at 37 °C.

2.3.5 Effects of Hexamer Conformation

In the presence of different allosteric molecules and ions, the insulin hexamer changes the conformation of 3-6 of its constituent monomers. These hexamer conformations–known as the T_6, T_3R_3, and R_6–have different 3D protein orientation and structure, and as such, most likely interact with each other differently in a model membrane at the air-water interface and in the body. Differences in the surface pressure-area compression isotherms for the zinc and copper insulin hexamer are shown below.

2.3.5.1 Zinc Insulin Hexamers

Surface pressure-area isotherms for the T_6, T_3R_3, and R_6 conformations of the zinc insulin hexamer are shown below in Figure 2.6.

Considered the "standard" insulin hexamer, the T_3R_3 conformation acts as our baseline insulin hexamer against which the other conformations have been compared. The T_6 insulin hexamer, shown in Figure 2.6, has a similar lift off area as the T_3R_3 conformation, but has a much lower collapse pressure and has a slight plateau region at about 30 mN/m. While also having a similar lift off molecular area to that of the T_3R_3, the R_6 differs as it has a slightly lower slope at surface pressures above 25 mN/m.

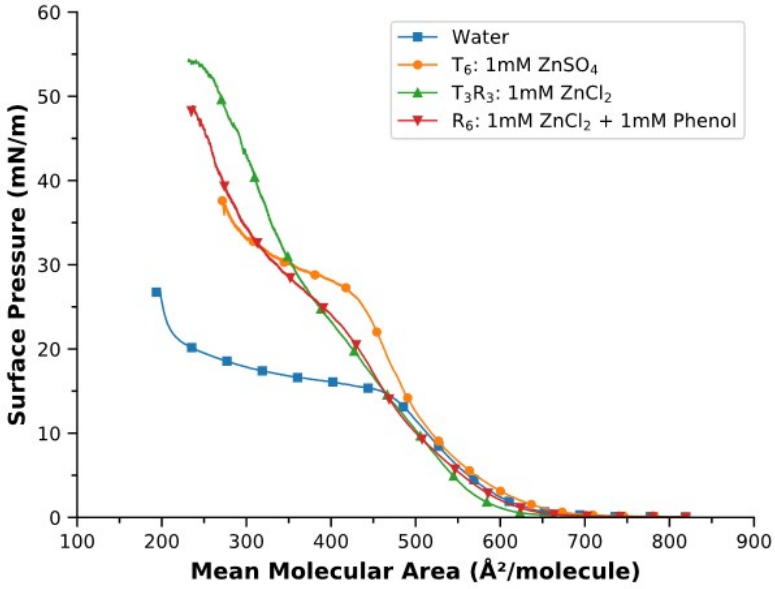

Figure 2.6: Surface Pressure-Area Isotherms Showing the Effect of Insulin Hexamer Conformation on Zinc

2.3.5.2 Copper Insulin Hexamers

Copper has also been studied previously by other researchers. The T_6 conformation of the copper insulin hexamer could not be attained in this research due to the precipitation of copper sulfate under physiological pH. The compression isotherms for the T_3R_3 and

R_6 copper insulin hexamers are shown in Figure 2.7. The lift off area (and subsequently the limiting molecular areas) for the T_3R_3 compression isotherm is lower than that of the R_6 indicating that the transition between the gas and liquid phases occurs as a lower area. This could be due to a decreased "readiness" of the T_3R_3 insulin hexamer to form the liquid phase, indicating that the liquid phase of the R_6 copper insulin hexamer is more stable as it more readily changes phase. This could, however, just be due to the increase side of the R_6 hexamer; the increase size would force the molecules to interact at a larger molecular area, though this is not displayed in the zinc insulin hexamer compression isotherms.

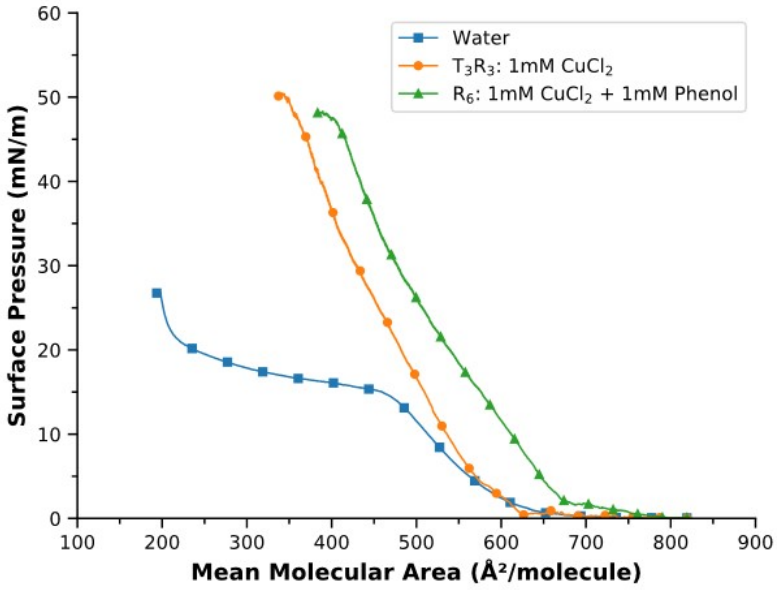

Figure 2.7: Surface Pressure-Area Isotherms Showing the Effect of Insulin Hexamer Conformation on Copper

2.3.6 Effects of Divalent Metal Cations

In order to more easily compare the differences between the zinc and copper insulin hexamers, the following graphs display the previously shown data but regrouped by the type of insulin hexamer conformation.

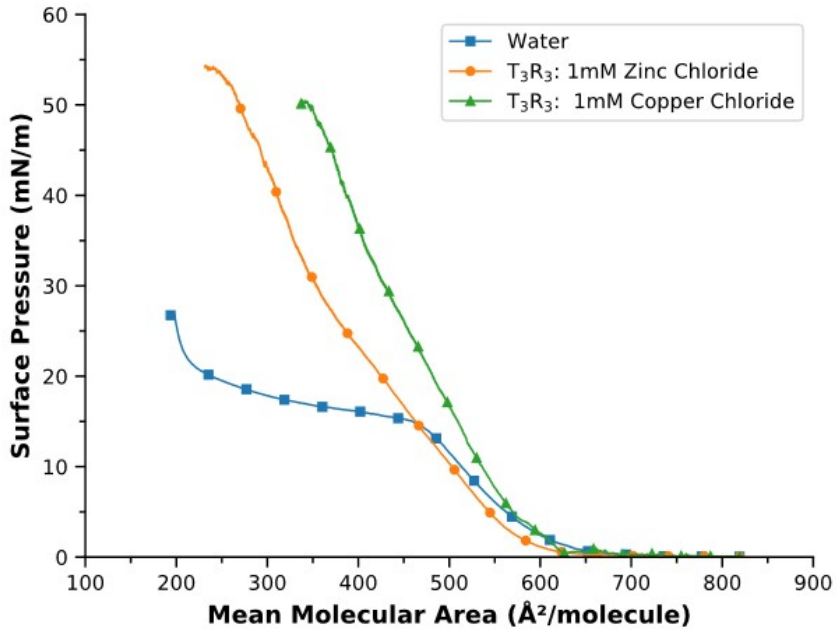

Figure 2.8: Surface Pressure-Area Isotherms Comparing the T_3R_3 Conformation of Zinc and Copper

It should be noted that one of the primary differences between the zinc and copper compression isotherms for both the T_3R_3 and the R_6 conformations is the lower limiting molecular area and shallower slope of the zinc insulin hexamer.

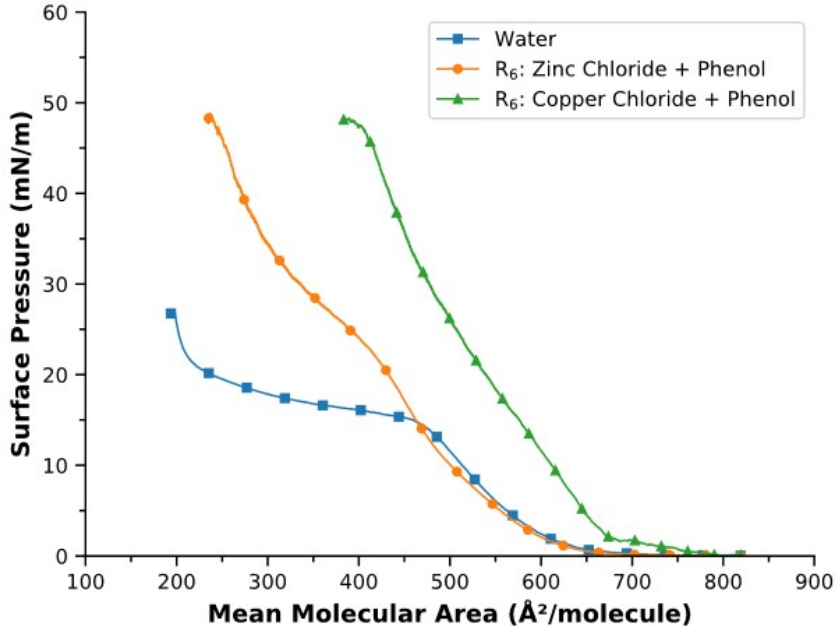

Figure 2.9: Surface Pressure-Area Isotherms Comparing the R_6 Conformation of Zinc and Copper

2.4 Conclusion

Overall, there seem to be slight, but noticeable, differences between the compression isotherms of not only the different insulin hexamer conformations, but also the different metal cations and compounds used. While we are still unsure of the actual differences in stability among all of these different insulin hexamers (additional hysteresis trials would help supplement this data and potentially allow us to determine the rough stability of each hexamer), this data does show that the Langmuir Monolayer technique can, in fact, differentiate between the momomeric and hexameric forms of insulin, between the different conformations of the insulin hexamer, and between the hexamers formed using different cations.

Chapter 3

Construction of a Brewster Angle Microscope

3.1 Previous Work

Brandon Allen, a past researcher in the Goach research group at Monmouth College, previously built a BAM using LEGO Mindstorms pieces following a published journal article.[45] His constructed BAM is is shown below in Figure 3.1.

The LEGO Mindstorms BAM was a novel attempt at producing a BAM, however, it fell short in the fact that it was never able to image monolayer films at the air-water interface. A sample image from this BAM is shown in Figure 3.2. While this seems like a BAM image at first (most notably due to the greyscale image and the diffracted artifacts within the image) most images looked exactly like this one: devoid of any true reflection from surfactants at the air-water interface. The most probably reason as to why this BAM failed to work was due to the optical setup. The optical components (the CCD camera and laser) shown in Figure 3.1 are placed on top of the mechanical arms. This induces height above the plane of rotation in the arms and, therefore, eliminates the BAM's ability to adjust its angle while keeping all of the optical components in line with each other.

After deliberation, it was determined that a new BAM need to be built using a sturdier, more professional material, as well as a new design to eliminate the optical components

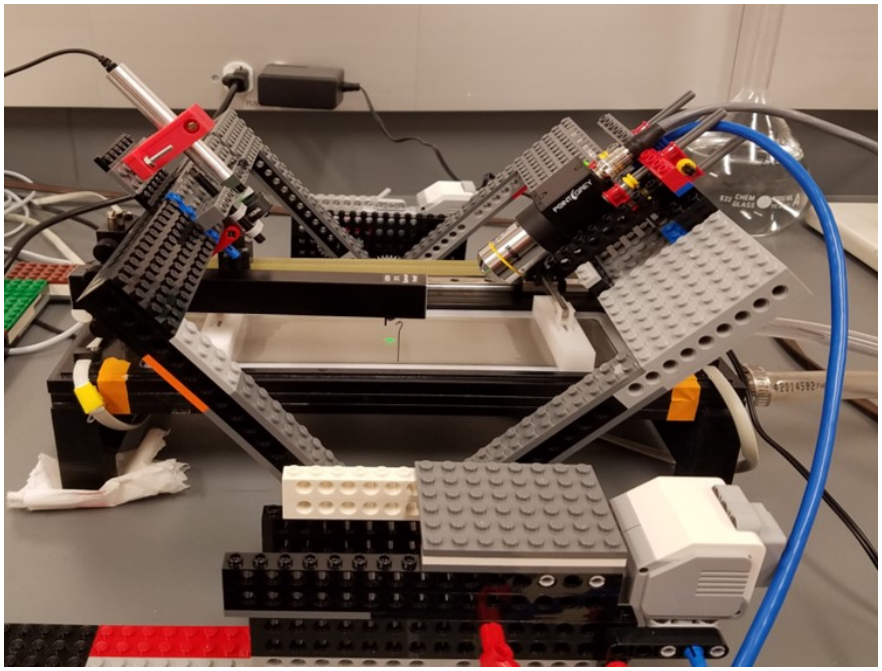

Figure 3.1: LEGO Mindstorms BAM constructed by Brandon Allen

residing on top of the support arms. This new design was to be built using metal extrusion and other mechanical parts which are screwed together to increase the regidity of the BAM and allow for increased accuracy when adjusting the angle of the arms.

3.2 Materials and Methods

The majority of materials for this build were purchased from OpenBuildsPartStore.[46] The components needed for this build have been broken down into two main sections: the Mechanical Assembly, which contains the design and parts necessary to construct the main frame of the BAM, and the Optical Assembly, which contains the design and parts necessary for the acquisition of data from the BAM.

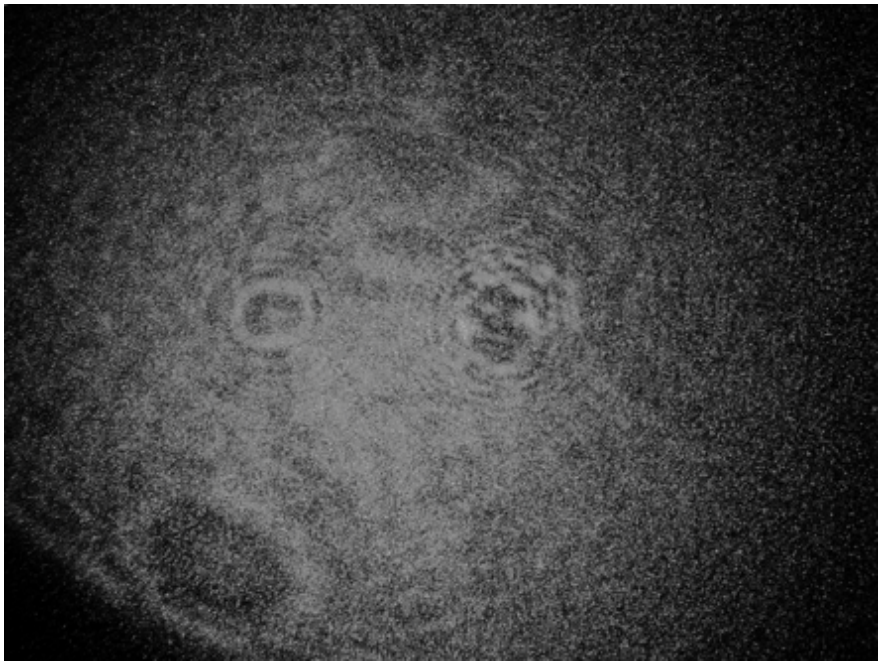

Figure 3.2: Sample BAM image from Brandon Allen's BAM

3.3 Mechanical Assembly

3.3.1 Frame

The initial design for the BAM was comprised of an all metal base and arms. This design is shown in Figure 3.3. The following is the parts list for the metal design:

- 20x80mm v-slot aluminum extrusion for the arm ends and base-plate
- Note: 20x80mm v-slot aluminum extrusion was used for the sides of the base
- 20x20mm v-slot aluminum extrusion for the vertical axis, arms, and arm connectors to the vertical angle adjuster
- Hidden/regular corner connectors were used to screw all fixed pieces together

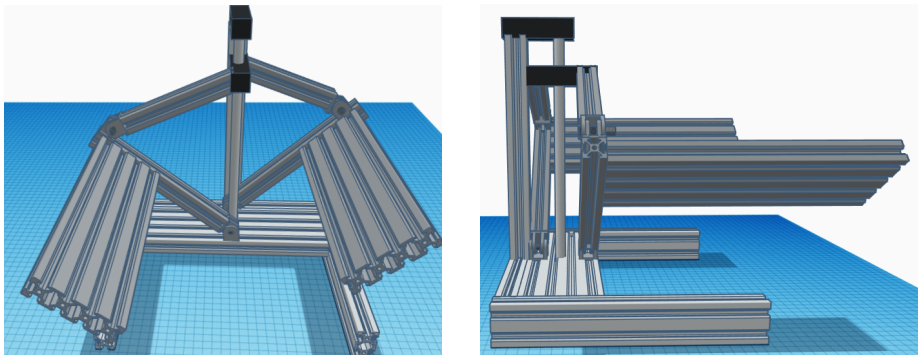

(a) Front Perspective **(b)** Side Perspective

Figure 3.3: Various perspectives for the initial 3D designed BAM

In order to use the regular corner connectors (which were used to connect the 80x20mm part of the arms to the 20mm part as well as the base plate to the base sides), the inner metal had to be threaded using a 5mm metal tap. This allowed for screws to be screwed into the metal to connect the pieces together. The hidden connectors slide into the v-slot groves and use an internal screw to tighten. Additionally, a set of rubber feet were placed on the bottom of the BAM to allow for stabilization and decrease the chances of the BAM sliding during a trial; one rubber foot was added to each corner of the base of the BAM. The majority of the pieces used for this part of the BAM are shown in Figure 3.4.

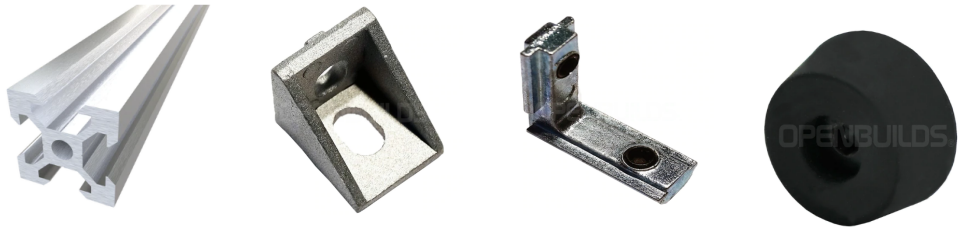

(a) V-Slot Metal Extrusion **(b)** Normal Corner Bracket **(c)** Hidden Corner Bracket **(d)** Rubber Foot

Figure 3.4: Various components used for the BAM frame

3.3.2 Arm Adjustment

In the previous BAM design made by Brandon Allen, the arms moved independently of each other. However, since the angle of incident light is exactly the same as the angle of reflected light, arms that move independently of each other are not required. By fixing both arms to the same point, movement of both arms is synchronous, removing additional error due to inconsistencies in the angles between the two arms.

In the new design for the BAM, the two arms are fixed to a piece of extrusion that moves up and down to adjust the angle of the arms. The components necessary for this are shown in Figure 3.5 and include:

- Acme screw set (300 mm T8 acme screw, copper screw nut, flexible coupler, and pillow bearing block)
- Gantry cart
- Nema 17 stepper motor
- Adjustable v-slot hinge

A piece of 20x80mm v-slot extrusion was connected to the gantry cart, which was placed on the vertical 20x20 v-slot metal extrusion. A hole was drilled into the base of the BAM to allow the Nema stepper motor to pass through. The acme screw was then attached to the stepper motor using the flexible coupler. The stepper motor was screwed into the base of the BAM using a mount shown in Figure 3.6. A small hole was then drilled into the metal extrusion connected to the gantry cart to allow the copper nut to fit inside (which the acme screw then threads inside of). The pillow bearing block was attached to the top of the acme screw and then placed into a mount shown in Figure 3.6.

(a) Acme Screw Set **(b)** Gantry Cart **(c)** Nema 17 Stepper Motor **(d)** Adjustable v-slot Hinge

Figure 3.5: Various components used for the BAM Arm Adjustment

3.3.3 3D Printed Components

In order for the BAM to be put together, several parts needed to be designed. First, a mounting plate needed to be made to mount the Nema stepper motor to the base of the BAM. Next, an acme screw mount was designed to hold the pillow bearing block and the acme screw. These parts were designed using the free online CAD software, tinkercad[47] and are shown in Figure 3.6

(a) Acme Screw Mount **(b)** Stepper Motor Mount

Figure 3.6: 3D Printed Parts for the Mechanical Assembly of the BAM

3.4 Optical Assembly

In order for the optical components to always be perfectly in line, they must exactly line up with a plane extending from the point of pivot; in this case, the optical components need to be aligned in the plane of the arms. To do this, mounts were made to hold the various optical components directly in the middle of the ends of the arms.

3.4.1 Optical Components

In order for a Brewster angle microscope to work, the incident light needs to be purely p-polarized when it strikes the surface of the water. In order to achieve this a polarizer is used and its transmission axis is lined up to produce p-polarized light from a laser source. The optical components used in the new BAM are as follows:

- PointGrey Flea3 GigE CCD camera
- Nikon plan N 10x/0.25 objective
- Thorlabs 4.6 mW Laser (532 nm)
- Linear nanoparticle polarizer
- Micromanipulator
- Linear actuator set
- Arduino stepper motor/driver
- Lab jacks

The laser light passes through the polarizer filtering out all but the p-polarized light. This light this strikes the subphase surface and reflects if there are surfactants present. The reflected light then passes through the 10x microscope objective, through another p-polarizer to ensure that ambient light is removed, and then goes to the CCD camera. In order for all of this to work, everything needs to be aligned. To help with the alignment of everything, a 1D micromanipulator was attached to the laser to allow for alignment with

the microscope/camera setup. Additionally, a custom linear actuator was designed to adjust the depth of the microscope/camera setup; the pieces of this actuator are shown in Figure 3.7 and the custom designed 3D components are shown in Figure 3.8 Additionally, lab jacks were used to raise and lower the surface of the subphase to align it with the pivot point of the arms.

Figure 3.7: Acme screw set utilized to build the custom linear actuator for microscope/camera setup. Parts in the set include an 8mm acme screw, dual support rods, pillow bearings, support blocks, and brass nut. The support rods and acme screw were cut to size and fitted into 3D printed mounts.

3.4.2 3D Printed Components

To mount the optical components to the BAM, several custom-designed 3D parts we needed. As with the 3D parts used in the mechanical assembly, these designs were made using Tinkercad. A camera mount was designed to hold the camera optics and mount it to the micromanipulator. Additionally a mount was designed to attach the micromanipulator to the BAM arm. Finally, a mount was designed and 3D printed to hold the

laser and polarizer and attach it to the micromanipulator. These 3D designs are shown in Figure 3.8.

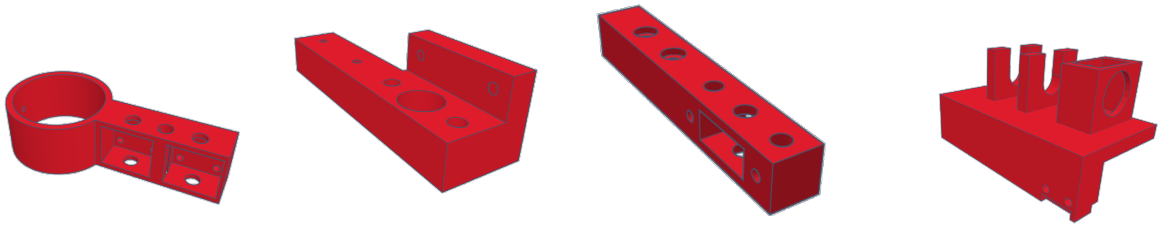

(a) Camera Mount **(b)** Left Actuator Mount **(c)** Right Actuator Mount **(d)** Laser Mount

Figure 3.8: 3D Printed Parts for the Optical Assembly of the BAM

3.5 Electrical Assembly

The entirety of the BAM build is controlled via LabVIEW software that interfaces with an Arduino Uno microcontroller. The Arduino Uno connects to two stepper motor drivers (INSERT TWO TYPES OF CONTROLLERS) which control the Nema 17 stepper motor, used to control the BAM arms, and the small reduction stepper motor, used to control the linear actuator for the objective/camera. The wiring diagram for the electrical assembly is shown in Figure (INSERT FIGURE REFERENCE).

INSERT IMAGE SCHEMATIC OF WIRING

3.6 Final Build

With both the mechanical and optical assembly prepared, the BAM was finished and ready to be tested. The final design is shown in Figure 3.9

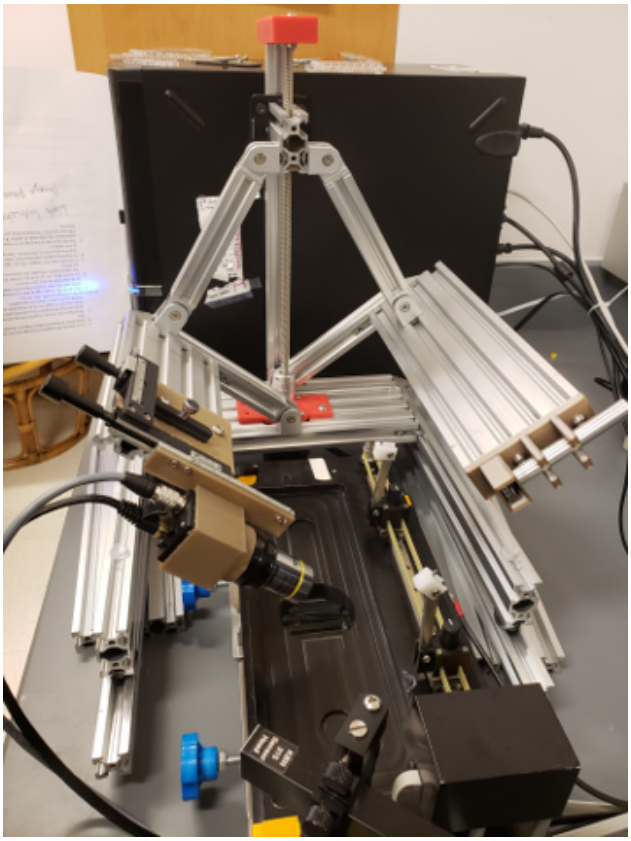

Figure 3.9: Final design of the new BAM

3.7 Preliminary Results

Initial testing of the BAM was performed using a 3D printed trough tray coated with wax that had an increased depth of water. This allowed for increased distance between the reflected light from the surface and light reflected from the bottom of the trough tray. However, do to the increased height of water, and therefore, increase height of the trough tray, the barriers on the Kibron trough would not fit. In order to compress the monolayer, a manual compression was used whereby the trough barriers were placed on top of the trough tray and pressed together by hand. In addition, the Kibron trough pressure sensor

was not used during these trials.

A series of trials were performed to test the BAM setup and visualize miscellaneous film morphologies. In each image there is only one line that is in focus due to the oblique viewing angle of the microscope objective and camera. The rest of the image is slightly distorted and shows large diffraction artifacts due to this.

3.7.1 Cholesterol

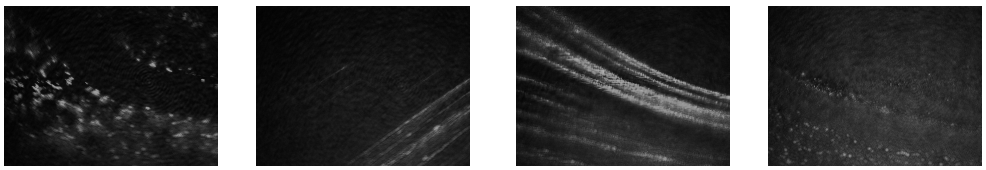

(a) **(b)** **(c)** **(d)**

Figure 3.10: Preliminary BAM Images of Cholesterol at Various Areas

3.7.2 DPPC

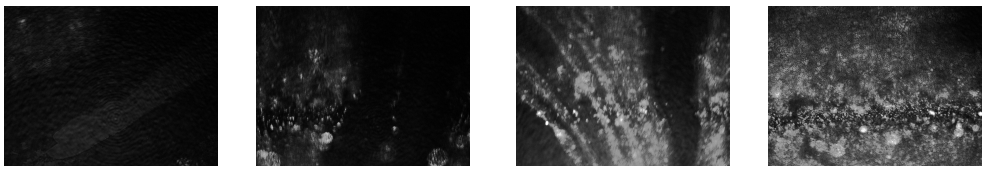

(a) **(b)** **(c)** **(d)**

Figure 3.11: Preliminary BAM Images of DPPC at Various Areas

3.7.3 DPPS

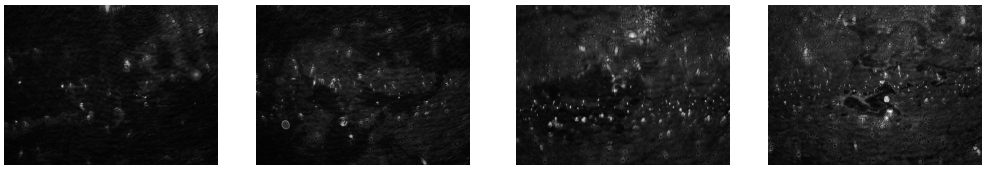

(a) **(b)** **(c)** **(d)**

Figure 3.12: Preliminary BAM Images of DPPS at Various Areas

3.7.4 DPPS and Cholesterol

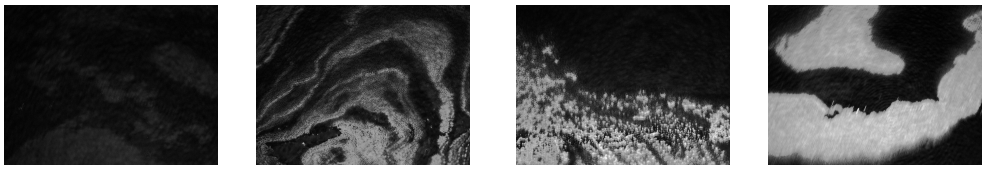

(a) **(b)** **(c)** **(d)**

Figure 3.13: Preliminary BAM Images of DPPS and Cholesterol at Various Areas

3.7.5 Insulin and Cholesterol

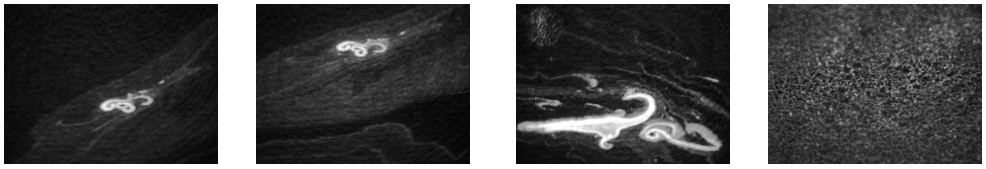

(a) **(b)** **(c)** **(d)**

Figure 3.14: Preliminary BAM Images of Insulin and Cholesterol at Various Areas

3.7.6 Insulin and DPPS

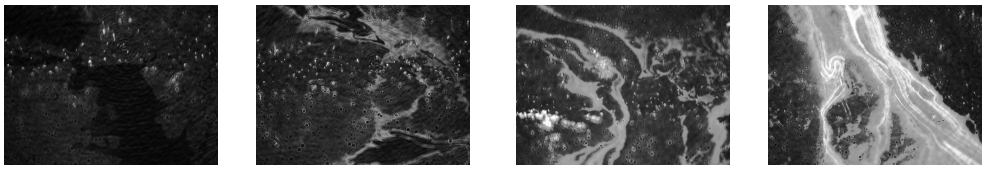

(a) **(b)** **(c)** **(d)**

Figure 3.15: Preliminary BAM Images of Insulin and DPPS at Various Areas

3.7.7 Insulin, DPPS, and Cholesterol

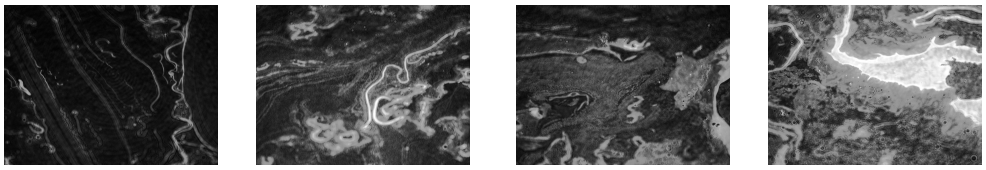

(a) **(b)** **(c)** **(d)**

Figure 3.16: Preliminary BAM Images of Insulin, DPPS, and Cholesterol at Various Areas

3.7.8 Insulin on $ZnCl_2$ Subphase

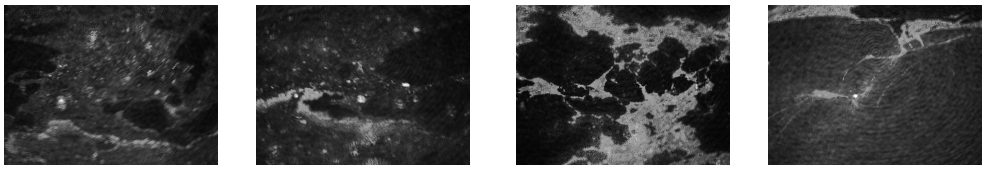

(a) **(b)** **(c)** **(d)**

Figure 3.17: Preliminary BAM Images of Insulin on $ZnCl_2$ at Various Areas

Chapter 4

Future Work

4.1 Insulin Project

The insulin project has long been a project in the Goach research lab, and as such has had numerous facets and changes over the years. The research presented herein focused primarily on the pH dependence of insulin and its aggregates as well as seeing how the different conformations of the insulin hexamer and various metal cations affected the stability of insulin. The following are idea that could directly supplement the work presented here.

- Some of the trials and data presented in this paper have not been reproduced in triplicate. The exact trials are listed in my (Seth Croslow) lab notebook. These trials could be completed to ensure that all of the data is correct and allow for us to state explicitly that all of the trials were performed in triplicate and averaged to produce the isotherms shown.

- The differences in divalent transition metal cations could continue to be explored by testing insulin with all of them (such as manganese, nickle, iron, etc.). These trials could all be done at various pH to study their affects at different pH and see if the results are the same among all the cations studied.

- To further assess the stability of the insulin hexamers, hysteresis trials of all of the trials presented here would be interesting. For this, the trials would simply needed to be repeated as presented here, however the student would use the hysteresis mode on the trough and see how the isotherms change during compression-relaxation cycles. This would give valuable insight into the differences in stability between the different metal cations as well as the different insulin hexamer conformations.

- The interactions with insulin and various constituent lipids of the cell membrane would be an interesting direction to take the project. The different conformations of insulin would be tested with lipids such as DPPC, cholesterol, DPPS, etc. to see what affect these lipids have on the state of the insulin (to potentially assess the efficacy of insulin injection into the body).

- As our studies typically study the aggregation of insulin, it would be interesting to focus on the dissociation of insulin aggregates. This could be accomplished in numerous ways. One way would be to perform hysteresis trials of insulin on a metal cation subphase and then slowly add a chelating agent (we have used EDTA successfully before) and see how that changes things. Additionally, you could start with hexameric insulin (zinc added to the insulin storage solution) and run trials with it on water (to see if it is still hexameric or if it dissociates under those conditions) and on a subphase of EDTA.

- Another interesting series of trials would be to do constant area trials of insulin (or constant pressure). You could apply a pure insulin solution to a subphase of water, start the trial, then add a divalent metal cation to see how the area changes. This could be done with all of the metal cations mentioned herein. Additionally, this

could be done in reverse: a hexameric insulin solution is added to a water subphase, then EDTA is injected into the subphase.

- Additional work could be done with the vanadium compounds. Additional compounds could be tested. Additionally, these trials could be performed under buffered conditions to maintain a constant pH throughout the entirety of the trial (a problem that we have had with current methods is a drastic change in pH during the trial leading to different speciation of the vanadium compounds).

- Finally, Brewster angle microscopy needs to be done of all the trials presented here, and could also be done for all of the project mentioned above. This would give valuable insight into the monolayer morhpology, phase composition, and structure during the trial.

4.2 Brewster Angle Microscope

The following sections details additional ideas, projects, and improvements that can be made on the *construction of a Brewster angle microscope* project. Some of these ideas would simply be nice changes to the BAM, while some are necessary to get a fully functioning BAM.

4.2.1 Design

Some of the additional changes and/or additions to the design of the BAM are as follows:

- Redesign some of the optics 3D prints (main optics mount and microscope objective mount) to fit more tightly and to help align the pieces better. Note: the objective mount is slightly off center, so the angled hole needs to be extended.

- The height of the BAM could be reduced by shortening the connections from the gantry cart to the BAM arm. This would help make the overall size of the BAM more compact and more easily movable.

- The hole of the main manipulator mount for the optics needs to be slightly tighter to prevent any movement of the brass nut during focusing of the camera. Additionally, the brass nut could be glued or screwed in.

- Spacers could be created to add between the hinges of the BAM to allow for tighter screwing of the hinges and to prevent any additional wobble in all of these joints.

- The main arm adjustment part of the BAM could be changed and improved by allowing the entire platform of the arms to raise and lower (enabling the user to focus the point of reflection on the trough exactly where it needs to be). Currently, this is done manually using lab jacks to raise and lower the trough, which is not very efficient.

- A housing needs to be created to hold all of the electronics for the BAM (the Arduino board, power supply, etc.) and a power button, power cable connector, and Arduino USB port could be added to make the BAM more complete.

4.2.2 Software

The following ideas are potential project and improvements that could be added/improved for the *construction of a Brewster angle microscope* project.

- Software needs to be made to control the angle of the BAM arms automatically. I attempted this, and have the mathematical derivation associated with a change in height of the gantry cart and relating it to a change in degrees. However, I was not able to fully implement this due to the fact that the LabView code utilized a 16 bit code and I needed more units of precision to allow for the total number of steps from 0 to Brewster's angle.

- Code needs to be written and implemented into the current LabView software to control the angle of the arms. One idea would just be an input box where you specify the angle you want, you have a current angle display, and an up and down adjustment button to increase or decrease the angle of the arms manually.

- The determination of Brewster's angle could also be determined automatically by increasing the angle of the arms and determining the total reflectance of the water subphase and then minimizing it. The angle where light is minimally reflected is the Brewster's angle for that subphase. This would be better than the current method as it would allow for the use of different subphases with different indices of refraction.

- LabView software needs to be written to automatically control the depth adjustment of the camera. In addition to this, a useful program would be to have the camera sweep forward and backward relatively fast as the camera takes pictures. The software could also implement a focus stacking method to create a single image that is fully in focus.

- Currently, the user has to go into the camera settings every time the BAM is turned on and set the correct settings that we use for the BAM trials. This should be able to be automatic by uploading the setting file from the camera into the LabView software such that the correct parameters would be set automatically.

- Finally, the BAM could easily be set up for quantitative Brewster angle microscopy. For reference, look at the Lego Brewster angle microscope paper by Fernsler et. al where they go into detail with all of the equations and processes to do this. They also have some published LabView code with thier methods for this (which could be easily altered to work with our BAM I believe).

4.2.3 Electronics

The following are ideas pertaining to the electronic systems of the BAM that could be created or improved.

- Electronic limit switches could be added to the arms of the BAM such that when the BAM starts, the arms could adjust to zero (hitting the limit switch and telling the BAM that the arms are at 0 degrees). This would allow for automatic and precice adjustment of the angle of the BAM arms.

- The stepper motors controlling the angle of the arms and the depth adjustment for the camera need to be wired together into the same Arduino board to allow for adjustment of both before and during a trial. Some software design would also probably have to accompany this.

Bibliography

(1) Mertens, J. Oil on Troubled Waters: Benjamin Franklin and the Honor of Dutch Seamen. *Physics Today* **2006**, 36–41.

(2) Wang, D.-N.; Stieglitz, H.; Marden, J.; Tamm, L. K. Benjamin Franklin, Philadelphia's Favorite Son, was a Membrane Biophysicist. *Biophysical Journal* **2013**, 287–291.

(3) Nepal, B.; Stine, K. J. Monolayers of Carbohydrate-Containing Lipids at the Water-Air Interface. *Cell Culture* **2019**.

(4) Masters, B. R. Lord Rayleigh: A Scientific Life. *Optics and Photonics News* **2009**, 37–41.

(5) Math, M. V.; Kattimani, Y. R.; Khadkikar, R. M.; Gadda, R. B.; Inamdar, R. S. Biophysics and Surface Chemistry in Physiology. *MGM Journal of Medical Sciences* **2015**, 149–152.

(6) Langmuir, I. The Constitution and Fundamental Properties of Solids and Liquids. Ii. Liquids.1. *Journal of the American Chemical Society* **1917**, 1848–1906.

(7) Vollhardt, D.; Fainerman, V. B. Phase transitions in Langmuir monolayers. *Colloids and Surfaces A: Physiochemical and Engineering Apsects* **2001**.

(8) Honig, D.; Mobius, D. Direct Visulization of Monolayers at the Air-Water Interface by Brewster Angle Microscopy. *The Journal of Physical Chemistry* **1991**.

(9) Nieto-Suarez, M.; Vila-Romeu, N.; Dynarowicz-Latka, P. Behavior of insulin-sphingomyelin mixed Langmuir monolayers spread at the air-water interface. *Colloids and Surfaces A: Physiochem. Eng. Aspects* **2008**.

(10) Grasso, E.; Oliveira, R.; Maggio, B. *Journal of Colloid and Interface Science* **2016**.

(11) Sessions, K.; Sacks, S.; Li, S.; Leblanc, R. M. epi-Fluorescence imaging at the air–water interface of fibrillization of bovine serum albumin and human insulin. *Chem. Commun.* **2014**.

(12) Stottrup, B. L.; Nguyen, A. H.; Tuzel, E. Taking another look with fluorescence microscopy: Image processing techniques in Langmuir monolayers for the twenty-first century. *Biochemica et Biophysica Acta (BBA)-Biomembranes* **2010**.

(13) Stine, K. J.; Whitt, S. A.; Uang, J. Y.-J. Fluorescence microscopy study of Langmuir monolayers of racemic and enantiomeric N-stearoyltyrosine. *Chemistry and Physics of Lipids* **1993**.

(14) Modinska, A.; Bauman, D. The Langmuir-Blodgett Technique as a Tool for Homeotropic Alignment of Fluorinated Liquid Crystals Mixed with Arachidic Acid. *International Journal of Molecular Sciences* **2011**.

(15) De Meyer, F.; Smit, B. Effect of cholesterol on the structure of a phospholipid bilayer. *PNAS* **2009**.

(16) Tuin, G.; Stein, H. N. The Excess Gibbs Free Energy of Adsorption of Sodium Dodecylbenzenesulfonate on Polystyrene Particles. *Langmuir* **1994**.

(17) Savva, M.; Acheampong, S. The Interaction Energies of Cholesterol and 1,2-Dioleoyl-snGlycero-3-Phosphoethanolamine in Spread Mixed Monolayers at the Air-Water Interface. *Journal of Physical Chemistry B* **2009**.

(18) Fu, Z.; Gilbert, E. R.; Liu, D. Regulation of Insulin Synthesis and Secretion and Pancreatic Beta-Cell Dysfunction in Diabetes. *Current Diabetes Reviews* **2013**.

(19) http://watcut.uwaterloo.ca/webnotes/Metabolism/Hormones.htmlhormonesInsulinwatcut.com.

(20) Liu, W.; Johnson, S.; Micic, M.; Orbulescu, J.; Whyte, J.; Garcia, A. R.; Leblanc, R. M. Study of the Aggregation of Human Insulin Langmuir Monolayer. *Langmuir* **2012**.

(21) Weiss, M.; Steiner, D. F.; Philipson, L. H. Insulin Biosynthesis, Secretion, Structure, and Structure-Activity Relationships. *NCBI Bookshelf* **2014**.

(22) Prugovečki, B.; Ivetić, N.; Matković-Čalogović, D. Crystal Structure of the Cobalt Human Insulin Derivative. *Macedonian Journal of Chemistry and Chemical Engineering* **2015**.

(23) Berchtold, H.; Hilgenfeld, R. Binding of Phenol to R_6 Insulin Hexamers. *Biopolymers (Peptide Science)* **1999**.

(24) Lisi, G. P.; Png, C. Y. M.; Wilcox, D. E. Thermodynamic Contributions to the Stability of the Insulin Hexamer. *Biochemistry* **2014**.

(25) Brewster, D. Experiments on the depolarisation of light as exhibited by various mineral, animal, and vegetable bodies, with a reference of the phenomena to the general principles of polarisation. *Royal Chemical Society* **1815**.

(26) Hénon, S.; Meunier, J. Microscope at the Brewster angle: Direct observation of first-order phase transitions in monolayers. *Review of Scientific Instruments* **1991**.

(27) Meunier, J. Why a Brewster angle microscope? *Colloids and Surfaces A: Physicochemical and Engineering Aspects* **2000**.

(28) Lisgarten, D.; Palmer, R.; Lobley, C.; Naylor, C.; Chowdhry, B.; Al-Kurdi, Z.; Badwan, A.; Howlin, B.; Gibbons, N.; Saldanha, J. Ultra-High Resolution X-Ray Structures of Two Forms of Human Recombinant Insulin at 100K. *Chemistry Central Journal* **2017**.

(29) Roder, P.; Liu, Y; W., H. Pancreatic Regulation of Glucose Homeostasis. *Experimental Molecular Medicine* **2016**.

(30) Antolikova, E.; Zakova, L.; Turkenburg, J.; Watson, C.; Hanclova, I.; Sanda, M.; Cooper, A.; Kraus, T.; Brzozowski, A.; Kiracek, J. Non-Equivalent Role of Inter- and Intramolecular Hydrogen Bonds in the Insulin Dimer Interface. *Journal of Biological Chemistry* **2011**.

(31) Raja, U.; Injeti, S.; Culver, T.; McCabe, J.; Angel, L. Probing the Stability of Insulin Oligomers Using Electrospray Ionization Ion Mobility Mass Spectrometry. *European Journal of Mass Spectrometry* **2015**.

(32) Rahuel-Clermont, S.; French, C.; Kaarsholm, N.; Dunn, M. Mechanisms of Stabilization of the Insulin Hexamer through Allosteric Ligand Interactions. *Journal of Biochemistry* **1997**.

(33) Hodgkin, D. X Rays And the Structure of Insulin. *British Medical Journal* **1971**.

(34) Ciszak, E.; Smith, G. Crystallographic Evidence for Dual Coordination Around Zinc in the T3R3 Human Insulin Hexamer. *Biochemistry* **1994**.

(35) Smith, G.; Swenson, D.; Dodson, E.; Dodson, G.; Reynolds, C. Structural Stability in the 4-Zinc Human Insulin Hexamer. *Proceedings of the National Academy of Sciences of the United States of America* **1984**.

(36) Roy, M.; Brader, M.; Lee, R.; Kaarsholm, N.; Hansen, J; Dunn, M. Spectroscopic Signatures of the T to R Conformational Transition in the Insulin Hexamer. *Journal of Biological Chemistry* **1989**.

(37) Chang, X.; Jorgensen, A.; Bardum, P.; Led, J. Solution Structures of the R6 Human Insulin Hexamer. *Biochemistry* **1997**.

(38) Carpenter, M.; Wilcox, D. Thermodynamics of Formation of the Insulin Hexamer: Metal-Stabilized Proton-Coupled Assembly of Quaternary Structure. *Biochemistry* **2014**.

(39) Derewenda, U.; Derewenda, Z; Dodson, E.; Dodson, G.; Reynolds, C.; Smith, G.; Sparks, C.; Swenson, D. Phenol Stabilizes More Helix in a New Symmetrical Zinc Insulin Hexamer. *Nature* **1989**.

(40) Gavrilova, J.; Tougu, V.; Palumaa, P. Affinity of Zinc and Copper Ions for Insulin Monomers. *Metallomics* **2014**.

(41) Brader, M.; Borchardt, D.; Dunn, M. The T to R Transition in the Copper(II)-Substituted Insulin Hexamer. Anion Complexes of the R-State Species Exhibiting Type 1 and Type 2 Spectral Derivative. *Biochemistry* **1992**.

(42) Prugovecki, B.; Ivetic, N.; Matkovic-Calgovic, D. Crystal Structure of the Cobalt Human Insulin Derivative. *Macedonian Journal of Chemistry and Chemical Engineering* **2015**.

(43) Nieto-Suarez, M.; Vila-Romeu, N.; Prieto, I. Behaviour of Insulin Langmuir Monolayers at the Air-Water Interface under Various Conditions. *Thin Solid Films* **2008**.

(44) Lord, R.; Gubensek, F.; Rupley, J. Insulin Self-Association. Spectrum Changes and Thermodynamics. *Biochemistry* **1973**.

(45) Fernsler, J.; Nguyen, V.; Wallum, A.; Benz, N.; Hamlin, M.; Pilgram, J.; Vanderpoel, H.; Lau, R. A LEGO Mindstorms Brewster angle microscope. *American Journal of Physics* **2017**.

(46) https://openbuildspartstore.com/.

(47) https://www.tinkercad.com/.